J. Fluid Mech. (2025), *vol.* 1019, R3, doi:10.1017/jfm.2025.10594

Rotation-induced vibrations of a cylinder in quiescent fluid

Rémi Bourguet

Institut de Mécanique des Fluides de Toulouse, Université de Toulouse and CNRS, Toulouse 31400, France
Corresponding author: Rémi Bourguet, remi.bourguet@imft.fr

(Received 19 May 2025; revised 16 July 2025; accepted 3 August 2025)

The present work brings to light the vibrations emerging when a circular cylinder, elastically mounted along a rectilinear path in quiescent fluid, is subjected to a forced rotation about its axis. These rotation-induced vibrations (RIV) are explored numerically for ranges of the four governing parameters. The Reynolds number and the reduced velocity (inverse of the non-dimensional natural frequency of the oscillator), based on the surface velocity of the rotating body and its diameter, are varied up to 100 and 250, respectively, and the structural damping ratio up to 50 %. The structure to displaced fluid mass ratio ranges from 0.1 to 1000. Vibrations are found to occur over a vast region of the parameter space, including the four orders of magnitude of the mass ratio under study, and high levels of structural damping. The amplitude of RIV may exceed 30 body diameters, while their frequency varies and deviates from the oscillator natural frequency, even though it is always lower. Despite its simplicity and the steady nature of the actuation, the system exhibits a considerable diversity of behaviours. Three distinct RIV regimes are encountered: two periodic regimes whose responses differ by their spectral contents, i.e. sinusoidal versus multi-harmonic, and an aperiodic regime. These regimes are all closely connected to flow unsteadiness, in particular via the interplay of the cylinder with previously formed vortices, which persist in the vicinity of the body.

Key words: flow-structure interactions, vortex shedding

1. Introduction

A circular cylinder mounted on an elastic support and placed in a cross-current represents a paradigm to study vortex-induced vibrations (VIV), a phenomenon ubiquitous in nature and with direct impact on the fatigue life of engineering structures (Williamson &

Govardhan 2004). Such vibrations are driven by a synchronisation of cylinder motion and flow unsteadiness associated with vortex formation in the wake. They exhibit peak amplitudes of the order of one body diameter in the cross-flow direction. A forced rotation applied to the elastically mounted cylinder breaks the symmetry of the system and may substantially alter its behaviour (Stansby & Rainey 2001; Yogeswaran & Mittal 2011; Bourguet & Lo Jacono 2014; Zhao, Cheng & Lu 2014; Seyed-Aghazadeh & Modarres-Sadeghi 2015; Wong *et al.* 2017; Bourguet 2020, 2023). Among other aspects, the rotation was found to enhance body oscillations and trigger a transition to another form of responses, referred to as galloping-like, whose magnitude, in contrast to VIV, increases unboundedly with the reduced velocity, i.e. the inverse of the oscillator natural frequency non-dimensionalised by the cylinder diameter and the current velocity.

Considering the influence of the forced rotation on VIV, in particular their amplification, the question that arises is whether a cross-current is actually required for the rotating cylinder to vibrate. In other words, can the rotation lead to structural oscillations for a body placed in quiescent fluid? The observations reported in a recent work concerning a rotating cylinder free to translate along a rectilinear trajectory, without structural restoring force, suggest that this is indeed the case (Bourguet 2025): irregular oscillations of amplitudes exceeding ten diameters, named saccades, were detected when the cylinder drifts at the current velocity, and the relative flow seen by the body thus vanishes. The vibrations developing in quiescent fluid under the effect of a forced rotation remain to be investigated for an elastically mounted cylinder. These 'rotation-induced vibrations' (RIV) are the object of the present study.

This work examines a novel facet of the interactions encountered in quiescent fluid, due to an actuation of the body. Beyond the fundamental aspects addressed hereafter, it could have implications for applications (e.g. mixing). In prior studies, the actuation often consisted in a forced oscillation of the cylinder, which relates to the problem of flexible structures exposed to oscillatory flows or waves (Sumer & Fredsøe 1988; Anagnostopoulos & Iliadis 1998; Fernandes, Mirzaeisefat & Cascao 2014; Dorogi, Baranyi & Konstantinidis 2023). Here, the actuation of the cylinder, elastically mounted along a rectilinear path, is a steady rotation. The surface velocity of the body is used, together with its diameter, to define the Reynolds number and the reduced velocity. The two other governing parameters are the structure to displaced fluid mass ratio and the structural damping ratio. The parameter space is explored on the basis of numerical simulations, in order to propose a first global vision of the fluid–body system behaviour, and shed some light on the physical mechanisms involved in the development of RIV.

2. Formulation and numerical method

A sketch of the physical system is presented in figure 1(*a*). The circular cylinder of diameter D and mass per unit length M_c is parallel to the z axis. It is mounted on an elastic support of structural stiffness per unit length k, and damping per unit length d, and is free to translate along the y axis within a quiescent fluid of density ρ_f and viscosity μ. The cylinder is subjected to a forced, anticlockwise, steady rotation of angular velocity Ω, about its axis. All the physical variables are non-dimensionalised by ρ_f, D, and the body surface velocity $U = \Omega D/2$. The cylinder displacement, non-dimensionalised by D, is denoted by ζ. The tangential force coefficient is defined as $C = 2F/(\rho_f D U^2)$, where F is the dimensional fluid force per unit length aligned with the direction of motion (y axis). The dynamics of the cylinder is governed by the equation

$$\ddot{\zeta} + \frac{4\pi\xi}{U^\star}\dot{\zeta} + \left(\frac{2\pi}{U^\star}\right)^2 \zeta = \frac{2C}{\pi m^\star}, \tag{2.1}$$

(*a*)

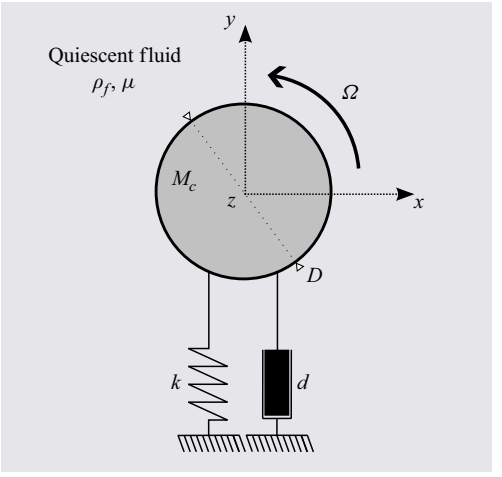

(*b*)

Peak force coefficient (forced oscillation)

Study	(*Re*, *KC*) (100, 8)	(180, 4.5)	(250, 2.5)
Elston *et al.* (2006)	2.684	3.003	4.794
Koehler *et al.* (2015)	2.710	3.040	4.841
Present	2.690	3.044	4.851

(*c*)

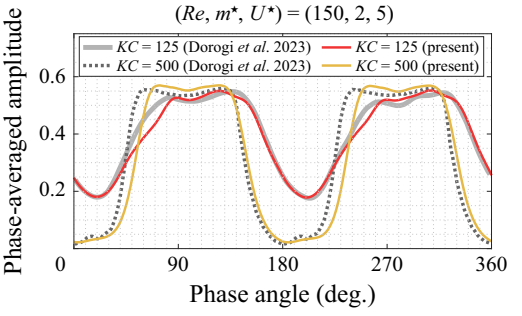

Figure 1. (*a*) Sketch of the physical system. (*b*) Peak value of the tangential force coefficient exerted on a non-rotating cylinder forced to oscillate in quiescent fluid, for different values of *Re* and *KC*. (*c*) Phase-averaged amplitude of the displacement of an elastically mounted, non-rotating cylinder, subjected to an oscillatory flow / a forced oscillation in the perpendicular direction, for $(Re, m^\star, U^\star) = (150, 2, 5)$ and $KC \in \{125, 500\}$. For the validation cases, the peak velocity attained during the forced oscillation is used to normalise fluid force, and to define *Re*, *KC* and $U^\star$. The present results are compared to those reported by Elston, Blackburn & Sheridan (2006) and Koehler *et al.* (2015) in (*b*), and Dorogi *et al.* (2023) in (*c*).

where $\dot{}$ designates the non-dimensional time derivative. The structure to displaced fluid mass ratio, structural damping ratio, non-dimensional natural frequency and associated reduced velocity are defined as $m^\star = 4M_c/(\pi\rho_f D^2)$, $\xi = d/(2\sqrt{kM_c})$, $f_n = [D/(2\pi U)]\sqrt{k/M_c}$ and $U^\star = 1/f_n$, respectively.

The mass ratio ranges from 0.1 to 1000, and the reduced velocity is varied up to 250. Structural damping is introduced in specified cases, and set to zero otherwise. The Reynolds number $Re = \rho_f U D/\mu$ is kept below or equal to 100, which ensures that the flow remains two-dimensional over most of the parameter space. The three-dimensional transition is found to occur in the higher-*Re* range, typically above $Re = 75$. In the present work, as a first step, the flow dynamics is predicted by the two-dimensional Navier–Stokes equations throughout the parameter space. Three-dimensional simulation results indicate that the principal features of the system behaviour described hereafter persist beyond the transition.

The numerical method is the same as in previous studies concerning comparable systems (Bourguet 2020, 2023, 2025). It is briefly summarised, and some additional validation results are presented. The coupled flow–structure equations are solved by the parallelised code Nektar, which is based on the spectral/hp element method (Karniadakis & Sherwin 1999). The cylinder is placed at the centre of a large square computational domain (side length $600D$), which is discretised into 3975 spectral elements. A no-slip condition is applied on the cylinder surface, and a Neumann-type boundary condition is used on the external boundaries. Convergence studies were carried out to set the polynomial order to 4 and the non-dimensional time step to 0.005.

In order to validate the method in physical configurations close to the present one, comparisons with prior results concerning a non-rotating cylinder, either forced to oscillate

in quiescent fluid (Elston *et al.* 2006; Koehler *et al.* 2015), or elastically mounted in the direction normal to an oscillatory flow (Dorogi *et al.* 2023), are proposed in figure 1(*b*,*c*). In the latter configuration, the oscillatory flow is emulated by a forced oscillation of the cylinder along the x axis, while the body is free to move along the y axis. For these validation cases, the peak velocity attained during the sinusoidal oscillation is used as reference to normalise fluid force and to define the Reynolds number, Keulegan–Carpenter number (KC) and reduced velocity. The prescribed non-dimensional amplitude and frequency are equal to $KC/(2\pi)$ and $1/KC$, respectively. The peak value of the tangential force coefficient and the phase-averaged amplitude of the displacement match those reported in previous studies, which confirms the validity of the present numerical method.

Each simulation is initialised with the established flow past a rigidly mounted, rotating cylinder. Then the body is released with an initial velocity $\dot{\zeta} = 0.1$. The analysis is based on long time series collected after the initial transient dies out.

3. Fluid–body system behaviour

The rotating cylinder is found to vibrate over a wide region of the parameter space. Typical examples of RIV are visualised in figure 2, via time series of the displacement and associated frequency spectra. The selected cases, which are representative of the different regimes of the system, as shown in the following, depict a variety of behaviours in terms of regularity, amplitude and frequency content.

The properties of RIV are examined in the (Re, $U^\star$) domain for $m^\star = 1$ in figure 3; it is recalled that no structural damping is considered ($\xi = 0$), unless stated otherwise. In each plot, the region where the body vibrates is delineated by a solid line. It extends down to $Re \approx 4$ and $U^\star \approx 7$, and up to the largest values under study, $Re = 100$ and $U^\star = 250$. The vibration region is composed of two distinct zones of periodic responses (delimited by dashed lines and coloured in yellow in figure 3*a*), a first one (I) along the frontier of the vibration region, and a second one (II) that emerges further inside, and a vast area of aperiodic responses (coloured in grey). The same colour code is used in the spectra of figure 2 to specify the periodic/aperiodic nature of the responses. The cases selected in this figure are indicated by blue stars in figure 3(*a*). More generally, beyond vibration regularity, figure 3(*a*) maps the areas of periodic and aperiodic behaviours of the fluid–body system. This can be assessed by monitoring fluid velocity or force signals, as illustrated in figure 2(*a*), where C time series are also represented.

The time-averaged value of the displacement vanishes in all cases. The vibration amplitude is quantified by the averaged top 10 % of ζ (denoted by ζ_{10}). It tends to regularly increase with $U^\star$ (figure 3*b*). Some fluctuations can be noted as Re is varied, but the amplitudes reached in the higher-$U^\star$ range, of the order of $30D$, are much larger than VIV amplitudes (Williamson & Govardhan 2004), and are comparable to those reported for the saccades observed without structural restoring force (Bourguet 2025). The vibration frequency (f_ζ) refers to the frequency of the dominant component of the ζ spectrum, which is also its fundamental component in all periodic response cases. As shown in figure 3(*c*), the vibration frequency remains lower than the oscillator natural frequency throughout the vibration region, and the ratio f_ζ/f_n may attain very low values. To visualise this deviation, f_n is indicated in the spectra of figure 2 (green dash-dotted line). Such low frequency ratios also contrast with VIV typical trends. In the absence of structural damping and for the periodic responses, the condition $f_\zeta < f_n$ implies that the components of C and ζ at f_ζ are in phase. This phasing state is found to persist in the aperiodic response cases (figure 2*a*).

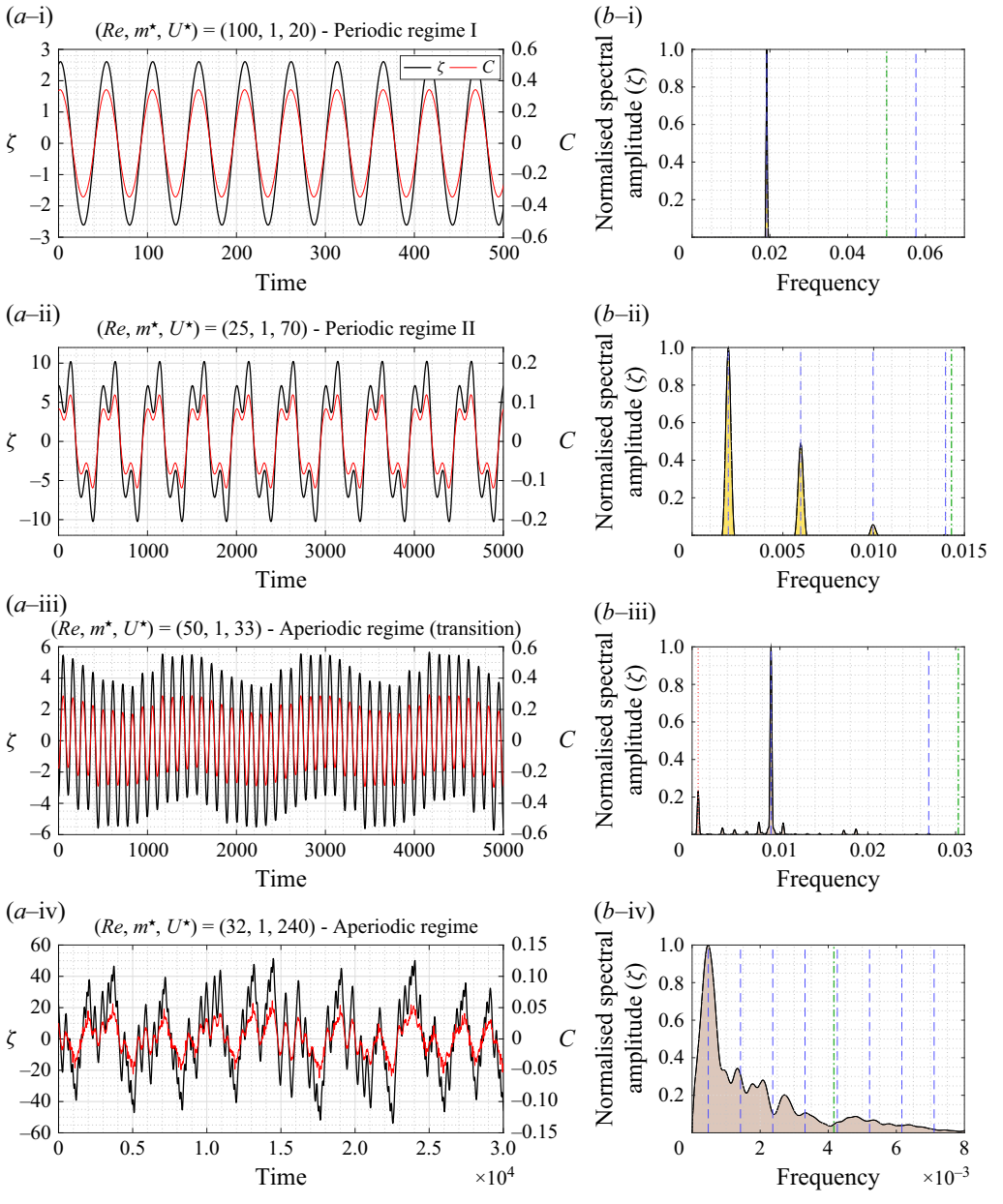

Figure 2. (*a*) Selected time series of the cylinder displacement and tangential force coefficient, and (*b*) frequency spectrum of the displacement, for (i) $(Re, m^\star, U^\star) = (100, 1, 20)$ (periodic regime I), (ii) $(Re, m^\star, U^\star) = (25, 1, 70)$ (periodic regime II), (iii) $(Re, m^\star, U^\star) = (50, 1, 33)$ (aperiodic regime, transition region), and (iv) $(Re, m^\star, U^\star) = (32, 1, 240)$ (aperiodic regime). In (*b*), the spectral amplitude is normalised by its maximum value; blue dashed lines denote the vibration frequency and its odd harmonics, and a green dash-dotted line represents the oscillator natural frequency. In (*b*–iii), the incommensurable component associated with the low-frequency modulation of the displacement is indicated by a red dotted line. The spectra are coloured according to the periodic (yellow) or aperiodic (grey) nature of the response.

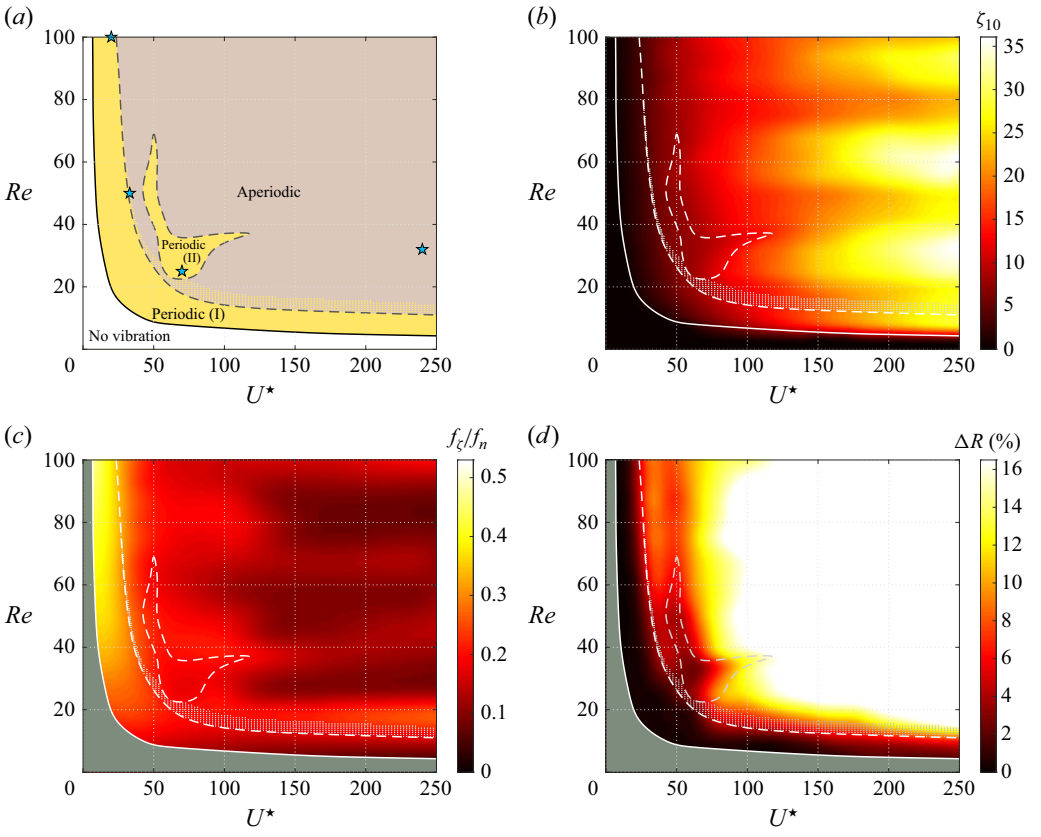

Figure 3. (*a*) Fluid–body system regime, (*b*) vibration amplitude, (*c*) vibration frequency normalised by the oscillator natural frequency, and (*d*) sinusoidal motion criterion (ΔR), as functions of the Reynolds number and reduced velocity, for $m^\star = 1$. The vibration region and, within this region, the zones where the system behaviour is periodic, are delimited by solid and dashed lines, respectively. The dotted area denotes the region of aperiodic behaviour where the response remains close to sinusoidal, with a slight low-frequency modulation. In (*a*), periodic and aperiodic behaviour regions are identified by yellow and grey background colours. Blue stars indicate the cases examined in figure 2.

The departure of the displacement signal from a harmonic oscillation is measured via the unsigned relative difference of the ratio $R = \zeta_{10}/\zeta_{RMS}$ with respect to the value expected for a sinusoidal response, denoted by ΔR, where ζ_{RMS} designates the root mean square value of ζ. The departure from harmonic evolution is particularly pronounced in the aperiodic response region (figure 3*d*). This criterion also highlights the distinct shapes of the vibrations occurring in each periodic response region: close to sinusoidal with higher harmonic contributions lower than 5 % of the fundamental component amplitude in region I, versus multi-harmonic with substantial higher harmonic contributions, typically third harmonic contributions larger than 25 % of the fundamental component amplitude, in region II. The examples in figure 2(*a*–i,*a*–ii,*b*–i,*b*–ii) depict these two forms of periodic responses. In all cases, only odd harmonic components (blue dashed lines in the spectra) contribute to the periodic responses. This symmetry of the oscillation betrays the symmetry of the organisation of the flow, which is discussed hereafter.

The strong sinusoidal nature of the vibrations in the periodic response region I persists beyond the edge of the aperiodic response region, in a transition zone denoted by a dotted area in the plots: the oscillation, still dominated by a single spectral component,

is modulated by a low-frequency, incommensurable component (red dotted line in figure 2*b*–iii). Beyond this transition zone, additional components progressively appear in the response spectrum, and the oscillation becomes increasingly erratic. Even though it is less clearly defined, a narrow zone of modulation can also be identified during the transition between the second periodic response region (II) and the aperiodic response region.

To recapitulate, RIV are found to develop through three regimes: two periodic regimes whose responses differ by their spectral contents, i.e. sinusoidal (periodic I) versus multi-harmonic (periodic II), and an aperiodic regime.

When the rotating cylinder does not vibrate, the flow surrounding it is steady. Body oscillation and flow unsteadiness arise simultaneously. The vibrations reflect the unstable nature of the fluid–body system, and the existence of oscillatory states where the equilibrium of the energy transfer between the fluid and the body is reached over each cycle ($1/f_\zeta$, periodic regimes), or over a longer time interval (aperiodic regime). The increasing trend of the amplitude with $U^\star$ is reminiscent of the quasi-steady mechanism driving, for example, the galloping oscillations of non-axisymmetric bodies (Modarres-Sadeghi 2022). In this case, the time scales of the flow and moving body are decoupled, and each step of body oscillation is seen as a steady configuration. As also observed for the galloping-like responses of a rotating cylinder in cross-current (Bourguet 2020, 2023), a quasi-steady modelling of fluid forcing, i.e. C replaced by its quasi-steady model in (2.1), fails to predict the present vibrations. This suggests that the interplay of the rotating cylinder and flow unsteadiness is important for the emergence of RIV.

The radial and azimuthal velocity components of the axisymmetric steady flow surrounding the non-vibrating cylinder are 0 and $D/(2\sqrt{x^2+y^2})$, respectively, i.e. circular Couette flow. Typical flows encountered in the different oscillatory regimes are visualised in figure 4 via series of snapshots of instantaneous spanwise vorticity. Flow dynamics essentially consists of an undulation, synchronised with body motion, of the vorticity layers wrapped around the cylinder. As the body oscillates, elongated zones of vorticity form in its wake, with the detachment of distinct vortices. The size of the vortical structures tends to increase as Re is decreased, of the order of D at $Re = 100$ (figure 4*a*), and one order of magnitude larger at $Re = 25$ (figure 4*b*).

In the absence of cross-current, the vortices are not convected away. They remain in the vicinity of the body until their diffusion, and may thus interact/collide with it during its subsequent oscillation cycles. The interaction with previously formed vortices may explain the development of irregular responses (aperiodic regime; figure 4*c*). This phenomenon was reported in oscillatory flow studies (Anagnostopoulos & Iliadis 1998; Dorogi *et al.* 2023). Despite the above-mentioned interaction, body motion and flow organisation can combine in such a way that the system dynamics is periodic. The number of vortices present close to the cylinder, and their arrangement, are expected to be important factors for the appearance of such dynamics. The periodic regimes exhibit persistent patterns: a single positive vortex is shed per half-cycle in the periodic regime I, versus two positive vortices of unequal sizes and magnitudes in the periodic regime II. The successively formed vortices are numbered in figure 4(*a*,*b*). The symmetry of these patterns during each half-cycle coincides with the symmetry of the cylinder displacement (odd harmonics only in the ζ spectrum).

To generalise the analysis, in figure 5, the behaviour of the system is examined over a range of mass ratios, at $Re = 50$. The distribution of the regimes previously identified for $m^\star = 1$, and the evolution of the vibration amplitude, across the ($m^\star$, $U^\star$) domain, are plotted in figure 5(*a*,*b*). The vibration region reaches the upper limit of the $U^\star$ range until

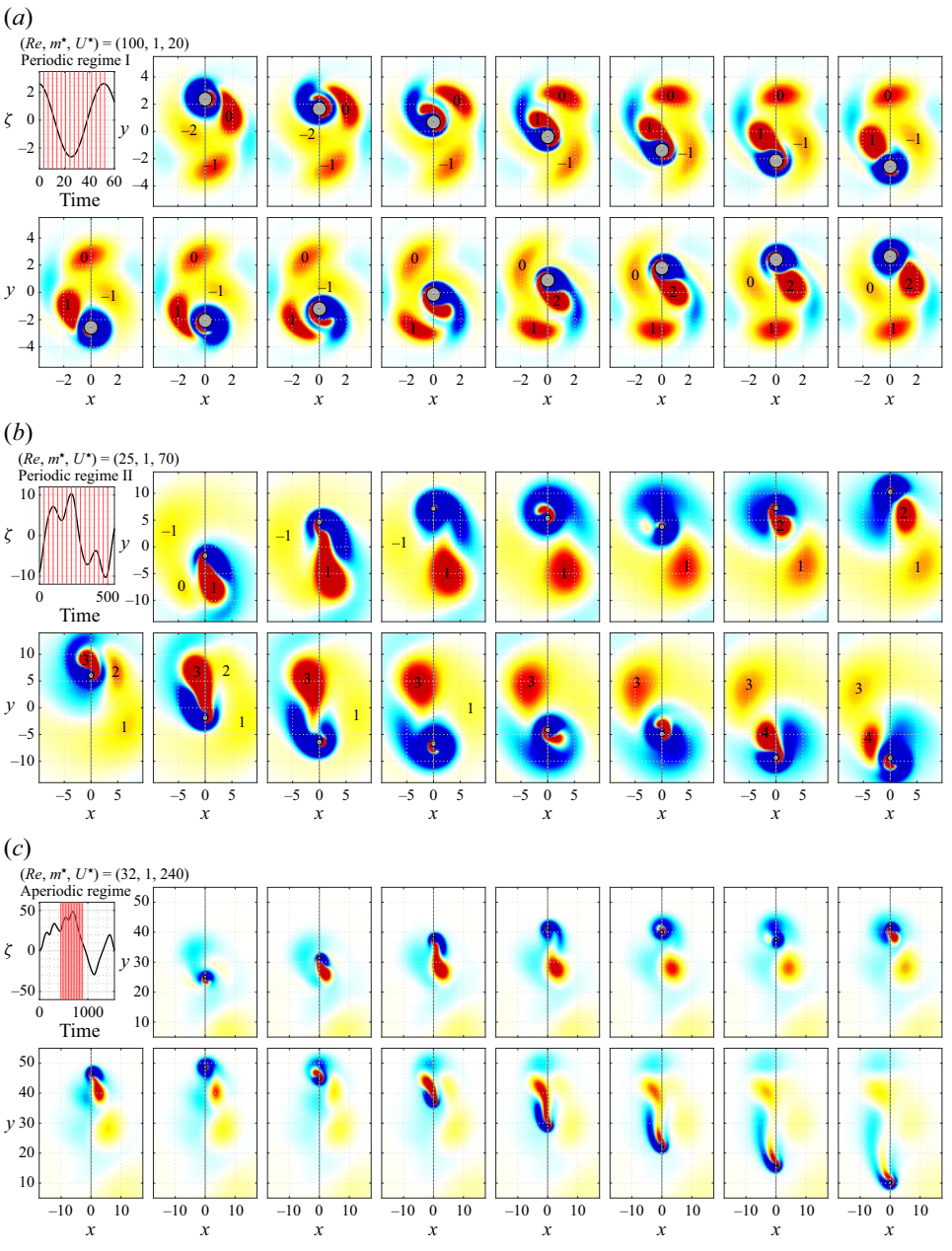

Figure 4. Selected time series of the cylinder displacement and instantaneous iso-contours of spanwise vorticity for (*a*) $(Re, m^\star, U^\star) = (100, 1, 20)$ (periodic regime I, $\omega_z \in [-0.075, 0.075]$), (*b*) $(Re, m^\star, U^\star) = (25, 1, 70)$ (periodic regime II, $\omega_z \in [-0.01, 0.01]$) and (*c*) $(Re, m^\star, U^\star) = (32, 1, 240)$ (aperiodic regime, $\omega_z \in [-0.02, 0.02]$). Positive/negative vorticity values are plotted in red/blue. The successive instants visualised in the snapshots are indicated by red lines in the time series. In (*a*,*b*), the positive vortices are numbered in their order of formation; number 1 corresponds to the first vortex formed during the sampling period.

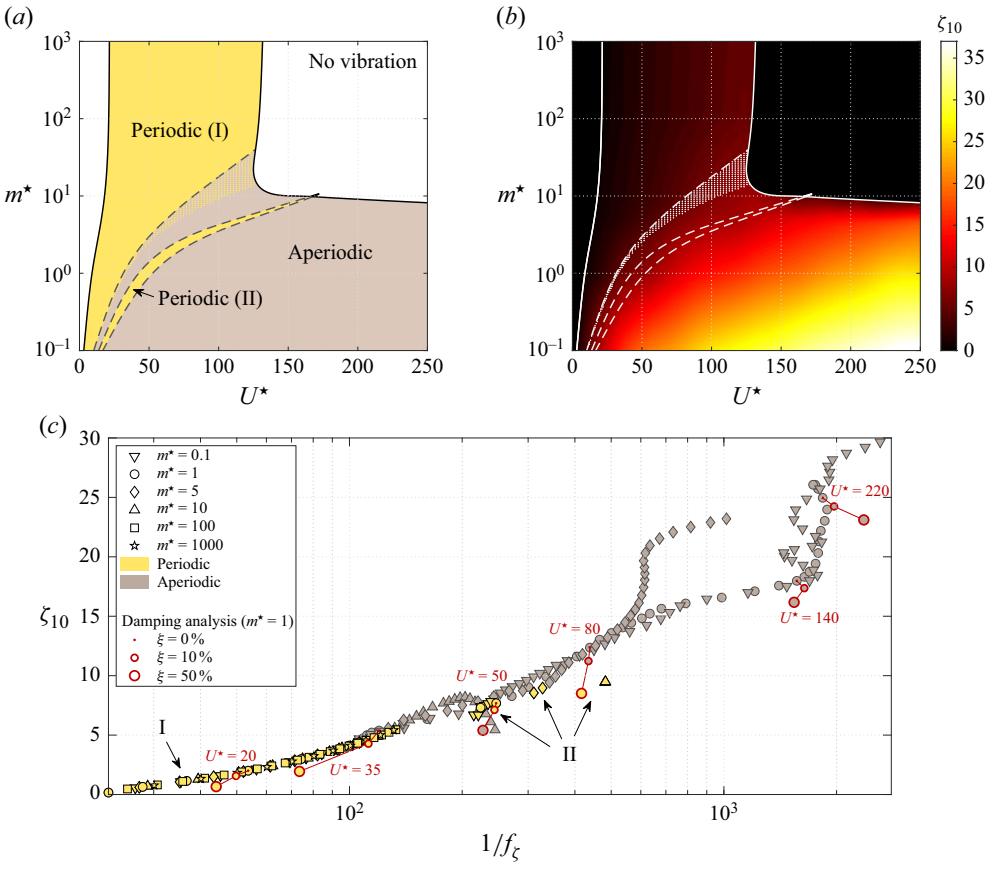

Figure 5. (*a*) Fluid–body system regime and (*b*) vibration amplitude, as functions of the mass ratio and reduced velocity, at $Re = 50$. The vibration region and, within this region, the zones where the system behaviour is periodic, are delimited by solid and dashed lines, respectively. The dotted area denotes the region of aperiodic behaviour where the response remains close to sinusoidal, with a slight low-frequency modulation. In (*a*), periodic and aperiodic behaviour regions are identified by yellow and grey background colours. (*c*) Vibration amplitude as a function of the vibration period ($1/f_\zeta$), for selected mass ratios ($Re = 50$). A range of reduced velocities is considered for each $m^\star$. The symbols are coloured according to the periodic or aperiodic nature of the system behaviour. The two forms of periodic behaviours (I and II) are specified in the plot. The results examined to study the impact of structural damping for $m^\star = 1$ are represented by red dots/circles ($\xi \in \{0\,\%,\ 10\,\%,\ 50\,\%\}$); the selected values of $U^\star$ are indicated in red.

$m^\star \approx 10$. It tends to shrink beyond, and the periodic regime II vanishes. The aperiodic regime, which dominates the $U^\star$ range for low $m^\star$, is observed until $m^\star \approx 40$. For higher $m^\star$ values, RIV develop for $U^\star \in [20, 130]$, through the periodic regime I. The peak amplitude versus $U^\star$ (close to $5D$) and, overall, the system behaviour, do not substantially vary with $m^\star$ any more. From a general perspective, low-$m^\star$ RIV are aperiodic and grow regularly with $U^\star$, while high-$m^\star$ RIV are mainly sinusoids of bounded magnitude. The vibration frequency (not plotted) remains lower than f_n but tends towards it as $m^\star$ is increased, e.g. $f_\zeta/f_n \in]0.99, 1[$ for $m^\star = 1000$.

A complementary visualisation of the response domain visited by the system is proposed in figure 5(*c*), which represents the vibration amplitude as a function of the vibration period ($1/f_\zeta$), over a range of $U^\star$ values, for selected mass ratios. The results obtained over four orders of magnitude of $m^\star$ follow comparable increasing trends, and tend to collapse

over a broad response range. The responses are particularly indiscernible in the periodic regime I, where body motion is close to sinusoidal. Such a coincidence is expected since under a sinusoidal oscillation assumption, a solution of the dynamics equation (2.1) for $(m^\star, U^\star)$ is also a solution of this equation for any other mass ratio, via an adjustment of the reduced velocity (Bourguet 2025).

To further extend the investigation, structural damping is introduced for $m^\star = 1$ and selected reduced velocities (red circles in figure 5*c*). An increase of the damping ratio from 0 % to 10 % and 50 % causes a reduction of the vibration amplitude. This reduction can be accompanied by a transition of regime, e.g. from the periodic regime II to the aperiodic regime for $U^\star = 50$, and the inverse for $U^\star = 80$. Yet the three regimes are found to persist for damped systems, and the trend of the responses in the amplitude/frequency domain remains globally the same as in the undamped cases.

The above observations illustrate the robustness of the phenomena uncovered in this work: RIV, and the distinct regimes through which they occur, exist over wide ranges of the different physical parameters.

4. Conclusions

In order to explore the emergence and underlying mechanisms of rotation-induced vibrations (RIV), the behaviour of the system composed of a circular cylinder, elastically mounted along a rectilinear path and forced to rotate about its axis, within a quiescent fluid, has been examined numerically, for ranges of the four governing parameters, i.e. Re and $U^\star$ up to 100 and 250, based on the body surface velocity, $m^\star \in [0.1, 1000]$ and $\xi \in \{0\,\%, 10\,\%, 50\,\%\}$.

Under the effect of the forced rotation, an oscillation of the cylinder arises, simultaneously with flow unsteadiness, over a vast region of the parameter space. This region encompasses the four orders of magnitude of the mass ratio considered in this work, and includes substantially damped systems. The amplitude of RIV may exceed 30 body diameters in the present parameter space. The vibration frequency varies and deviates from the oscillator natural frequency, but remains always lower than this frequency. Three regimes of RIV have been identified and mapped in the parameter space: two periodic regimes whose vibrations differ by their spectral contents, i.e. sinusoidal versus multi-harmonic, and an aperiodic regime. As an example, at $Re = 50$, low-$m^\star$ RIV are principally aperiodic and their amplitude increases regularly with $U^\star$, while high-$m^\star$ RIV are essentially sinusoids of bounded magnitude, occurring over a narrower interval of $U^\star$.

The vibrations are not predicted by a quasi-steady approach, which substantiates the importance of the interplay of the cylinder with flow unsteadiness in their development. Flow dynamics mainly consists of an undulation, synchronised with body motion, of the vorticity layers wrapped around the cylinder, with the formation of elongated zones of vorticity in its wake, and the detachment of distinct vortices. The size of the vortical structures depends on Re, but flow organisation exhibits persistent features. Each periodic regime is associated with a specific flow pattern, which matches body oscillation symmetry. The appearance of irregular responses (aperiodic regime) relates to the interaction of the cylinder with previously shed vortices.

To summarise, this work shows that a forced rotation applied to a cylinder, elastically mounted in quiescent fluid, can cause the body to vibrate. Two general aspects can be emphasised: (i) the robustness of RIV, as they are found to occur over broad ranges of the physical parameters; and (ii) the diversity of the behaviours of the fluid–structure system in the different RIV regimes, despite its simplicity and the steady nature of the actuation.

Funding. This work was performed using HPC resources from CALMIP (grants 2024-P1248, 2025-P1248).

Declaration of interests. The author reports no conflict of interest.

References

ANAGNOSTOPOULOS, P. & ILIADIS, G. 1998 Numerical study of the flow pattern and the in-line response of a flexible cylinder in an oscillating stream. *J. Fluids Struct.* **12**, 225–258.

BOURGUET, R. 2020 Two-degree-of-freedom flow-induced vibrations of a rotating cylinder. *J. Fluid Mech.* **897**, A31.

BOURGUET, R. 2023 Forced rotation enhances cylinder flow-induced vibrations at subcritical Reynolds number. *J. Fluid Mech.* **955**, R3.

BOURGUET, R. 2025 Rectilinear drift and oscillation of a rotating cylinder placed in flow. *J. Fluid Mech.* **1011**, A32.

BOURGUET, R. & LO JACONO, D. 2014 Flow-induced vibrations of a rotating cylinder. *J. Fluid Mech.* **740**, 342–380.

DOROGI, D., BARANYI, L. & KONSTANTINIDIS, E. 2023 Modulation and hysteresis in vortex-induced vibration of a spring-mounted cylinder in a slowly varying oscillatory stream. *J. Fluids Struct.* **122**, 103982.

ELSTON, J.R., BLACKBURN, H.M. & SHERIDAN, J. 2006 The primary and secondary instabilities of flow generated by an oscillating circular cylinder. *J. Fluid Mech.* **550**, 359–389.

FERNANDES, A.C., MIRZAEISEFAT, S. & CASCAO, L.V. 2014 Fundamental behavior of vortex self induced vibration (VSIV). *Appl. Ocean Res.* **47**, 183–191.

KARNIADAKIS, G.E. & SHERWIN, S. 1999 *Spectral/hp Element Methods for CFD*, 1st edn. Oxford University Press.

KOEHLER, C., BERAN, P., VANELLA, M. & BALARAS, E. 2015 Flows produced by the combined oscillatory rotation and translation of a circular cylinder in a quiescent fluid. *J. Fluid Mech.* **764**, 148–170.

MODARRES-SADEGHI, Y. 2022 *Introduction to Fluid–Structure Interactions*. Springer.

SEYED-AGHAZADEH, B. & MODARRES-SADEGHI, Y. 2015 An experimental investigation of vortex-induced vibration of a rotating circular cylinder in the crossflow direction. *Phys. Fluids* **27**, 067101.

STANSBY, P.K. & RAINEY, R.C.T. 2001 On the orbital response of a rotating cylinder in a current. *J. Fluid Mech.* **439**, 87–108.

SUMER, B.M. & FREDSØE, J. 1988 Transverse vibrations of an elastically mounted cylinder exposed to an oscillating flow. *J. Offshore Mech. Arctic Engng* **110**, 387–394.

WILLIAMSON, C.H.K. & GOVARDHAN, R. 2004 Vortex-induced vibrations. *Annu. Rev. Fluid Mech.* **36**, 413–455.

WONG, K.W.L., ZHAO, J., LO JACONO, D., THOMPSON, M.C. & SHERIDAN, J. 2017 Experimental investigation of flow-induced vibration of a rotating circular cylinder. *J. Fluid Mech.* **829**, 486–511.

YOGESWARAN, V. & MITTAL, S. 2011 Vortex-induced and galloping response of a rotating circular cylinder. In *IUTAM Symposium on Bluff Body Flows, IIT-Kanpur, India* (ed. S. Mittal & G. Biswas), pp. 153–156.

ZHAO, M., CHENG, L. & LU, L. 2014 Vortex induced vibrations of a rotating circular cylinder at low Reynolds number. *Phys. Fluids* **26**, 073602.